



Exploring the Performance Improvement of the Oxygen Evolution Reaction in a Stable Bimetal–Organic Framework System

Xiao-Li Wang⁺, Long-Zhang Dong⁺, Man Qiao⁺, Yu-Jia Tang, Jiang Liu, Yafei Li,^{*} Shun-Li Li, Jia-Xin Su, and Ya-Qian Lan^{*}

Abstract: Despite wide applications of bimetallic electrocatalysis in oxygen evolution reaction (OER) owing to their superior performance, the origin of the improved performance remains elusive. The underlying mechanism was explored by designing and synthesizing a series of stable metal–organic frameworks (MOFs: **NNU-21–24**) based on trinuclear metal carboxylate clusters and tridentate carboxylate ligands. Among the examined stable MOFs, **NNU-23** exhibits the best OER performance; particularly, compared with monometallic MOFs, all the bimetallic MOFs display improved OER activity. DFT calculations and experimental results demonstrate that introduction of the second metal atom can improve the activity of the original atom. The proposed model of bimetallic electrocatalysts affecting their OER performance can facilitate design of efficient bimetallic catalysts for energy storage and conversion, and investigation of the related catalytic mechanisms.

The oxygen evolution reaction (OER) plays a vital role in many alternative energy conversion technologies.^[1] Because of the sluggish kinetics caused by multistep four-electron transferring associated with O–H breaking and O–O formation, OER requires efficient electrocatalysts to overcome kinetic barriers and expedite the reaction.^[2] Over the past decades, owing to the superior catalytic performance, a number of bimetallic electrocatalysts for OER have been evaluated, including bimetallic oxides,^[3] hydroxides,^[4] phosphides,^[5] and chalcogenides.^[6] However, numerous bimetallic electrocatalysts are nanocomposites, whose performances are usually affected by many factors, such as particle size, morphology and synergistic effect.^[3b,7] Moreover, the mutual impact between the two kinds of metal remains elusive. In particular for some electrocatalysts with complicated components and poor crystallinity, the real phase cannot be precisely characterized, hampering the cross-validation between theoretical models and experimental results. These problems hinder the exploration and develop-

ment of novel bimetallic electrocatalysts.^[8] Consequently, defined structure and inter-metal interaction of a bimetallic electrocatalyst are essential for deciphering its performance improvement in OER.

Metal–organic frameworks (MOFs), as typical porous and crystalline materials composed by metal ions (or clusters) and organic linkers, have been widely investigated in recent years and proposed as potential catalysts.^[9] MOFs can be designed and tuned at the molecular level; the structure and coordination environment can be precisely determined by crystal X-ray crystallography. It is conducive to the theoretical prediction of electronic coupling and other interactions, thus facilitating the investigation of the reaction mechanism.^[9b,10] However, some MOFs are highly unstable when used as catalysts in certain reactions, such as hydrogen evolution reaction (HER), OER, and oxygen reduction reaction (ORR).^[11] To address chemical stability problems of MOFs, multiple approaches have been explored, including those using the high-valence metal ions and metal-ion metathesis.^[12] When carboxylates serve as the ligands, high-valent metal ions (for example, Fe³⁺, Al³⁺, Zr⁴⁺) are usually employed to strengthen the electrostatic interaction between the metal nodes and organic linkers.^[13] Among the high-valent metal ions, Fe-based compounds (for example, hydroxides, phosphides, nitrides) are widely investigated,^[14] and utilization of some Fe-based MOFs as electrocatalyst for OER were also reported recently.^[15] These investigations indicate that Fe-based MOFs are stable and active for OER. Therefore, Fe-based MOFs is a category of promising candidate for electrocatalysts compared with other classes of stable MOFs. If an iron atom in trinuclear Fe-cluster is replaced by a second atom, the structure of the resulting Fe₂M clusters will be similar to that of bimetallic electrocatalysts (for example, bimetallic oxides/phosphides/sulfides). Thus, the Fe₂M clusters can mimic bimetallic electrocatalysts and serve as the nodes that bridge organic ligands. Bimetallic MOFs produced by immobilizing the Fe₂M clusters in MOFs are expected to possess defined structure on the molecular scale, and thus are suited for studying the OER performance of bimetallic electrocatalysts in MOF system.

Herein, we designed and synthesized a series of MOFs based on Fe₂M(μ₃-O)(CH₃COO)₆(H₂O)₃ (Fe₂M, M = Fe, Co, Ni, Zn) clusters with the following considerations: 1) an iron atom in Fe₃ cluster can be replaced by a second metal with a similar radius that allows formation of Fe₂M clusters,^[13a,16] which is beneficial to realize the performance comparison of bimetallic electrocatalysts; 2) the preformed Fe₂M clusters are soluble and can maintain their structure and composition, which guarantees the formation of desired bimetallic MOF-

[*] X.-L. Wang,^[†] L.-Z. Dong,^[†] M. Qiao,^[†] Y.-J. Tang, Dr. J. Liu, Prof. Y. Li, Prof. S.-L. Li, J.-X. Su, Prof. Y.-Q. Lan
Jiangsu Collaborative Innovation Centre of Biomedical Functional Materials, Jiangsu Key Laboratory of New Power Batteries, School of Chemistry and Materials Science, Nanjing Normal University
No. 1, Wenyuan Road, Nanjing, 210023 (China)
E-mail: liyafei.abc@gmail.com
yqlan@njnu.edu.cn

[†] These authors contributed equally to this work.

Supporting information and the ORCID identification number(s) for the author(s) of this article can be found under:
<https://doi.org/10.1002/anie.201803587>.

based catalysts; and 3) the resulting bimetallic Fe_2M -MOFs feature enhanced chemical stability, satisfying the requirements of OER electrocatalysts. Accordingly, by bridging preformed Fe_2M clusters with biphenyl-3,4',5-tricarboxylic acid (BPTC) ligands, we prepared four isostructural Fe_2M -BPTC MOFs (Fe_3 -BPTC (**NNU-21**), Fe_2Co -BPTC (**NNU-22**), Fe_2Ni -BPTC (**NNU-23**) and Fe_2Zn -BPTC (**NNU-24**)). Among these stable MOFs, **NNU-23** exhibits the best OER performance with an overpotential of 365 mV at 10 mA cm^{-2} in 0.1M KOH, outperforming most previously reported MOF-based OER electrocatalysts. The experimental results reveal that the bimetallic MOFs possess the better OER activity than monometallic MOFs. Furthermore, the theoretical computation demonstrates that introduction of the second metal can make the d-band center close to the Fermi level and form a stronger binding interaction between the adsorbates and catalysts, thereby expediting OER process. This investigation offers thought for establishing precise bimetallic electrocatalysts and exploring the effect of the second metal on OER.

NNU-21–24 were synthesized by the reaction between preformed Fe_2M clusters and BPTC ligands under solvothermal conditions, with acetic acid serving as the competing reagent (see the Experimental Section in the Supporting Information). The optical microscope images (Supporting Information, Figure S3) and SEM images (Supporting Information, Figure S4) clearly show the similar morphologies of **NNU-21–24**. X-ray crystallographic analysis reveals that **NNU-21–24** are isostructural and crystallized in the tetragonal system with the $P4_12_12$ space group (**NNU-21–23**) and $P4_32_12$ space group (**NNU-24**), respectively (Supporting Information, Table S1). The preformed Fe_2M clusters contain two Fe^{III} ions, one M^{II} ion and one $\mu_3\text{-O}$, and are connected with six CH_3COO^- groups and three H_2O molecules (Supporting Information, Figure S1).^[13a] In **NNU-21–24**, the six CH_3COO^- groups of the clusters are completely substituted by COO^- groups from BPTC ligands, and each BPTC ligand connects three Fe_2M clusters (Supporting Information, Figure S2). Such a connection pattern is repeated to construct the 3D frameworks (Figure 1 a) and 3D channels (exemplified by **NNU-23** in Figure 1 b). Furthermore, topological analysis using TOPOS software suggests that **NNU-21–24** exhibit

a 3,6-c net topology (denoted as $\{6^{11}8^4\}\{6^3\}^2$ using Schläfli symbol).^[17] Figure 1c shows the natural tiling of **NNU-23**. Calculation by PLATON software reveals that the free volumes of **NNU-21–24** are 56.9%, 56.6%, 56.6%, and 56.7%, respectively.^[18]

The powder X-ray diffraction (PXRD) patterns of the as-synthesized **NNU-21–24** agree well with the simulated pattern derived from single crystal X-ray diffraction (Figure 2 a),

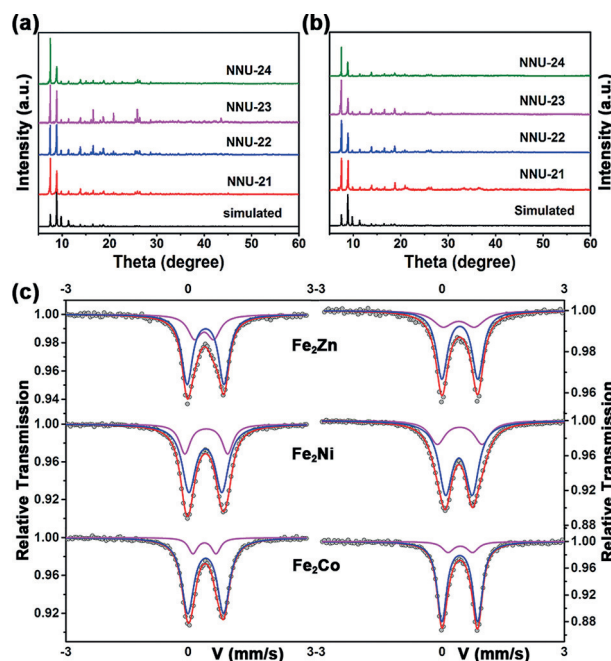


Figure 2. a) PXRD patterns of **NNU-21–24**, b) PXRD patterns of **NNU-21–24** immersed in 0.1 M KOH for 24 h, c) Mossbauer spectra for Fe_2M clusters (left) and the corresponding MOFs (right).

demonstrating their good crystallinity and high phase purity. To assess the chemical stability of these MOFs in electrolyte solution, we immersed 50 mg of crystals in 20 mL 0.1M KOH at room temperature. After 24 h, the pH of KOH solution changed slightly from 13.00 to 12.95, and the PXRD patterns (Figure 2b) remain unchanged. These results confirm the excellent stability of **NNU-21–24** in 0.1M KOH, and promise the utilization of these MOFs as OER electrocatalysts in alkaline medium. For Fe_2M ($\text{M} = \text{Co}, \text{Ni}, \text{Zn}$) clusters, previous reports determined the Fe/M stoichiometry as 2:1.^[13a] To verify the stoichiometry of Fe/M in **NNU-21–24**, we performed both energy-dispersive X-ray spectroscopy (EDS) (Supporting Information, Figure S6, Table S2) and inductively coupled plasma atomic emission spectroscopy (ICP-AES; Supporting Information, Table S3). The results confirm the 2:1 stoichiometry of Fe/M in **NNU-22–24**. Moreover, the ^{57}Fe Mossbauer spectra of Fe_2M -BPTC MOFs agree with that of Fe_2M cluster (Figure 2c), indicating that the composition of Fe_2M clusters is preserved upon formation of MOFs.

The thermal stability of **NNU-21–24** was evaluated by thermogravimetric analysis (TGA) under O_2 atmosphere, which reveals that **NNU-21–24** remain stable at ca. 350 °C

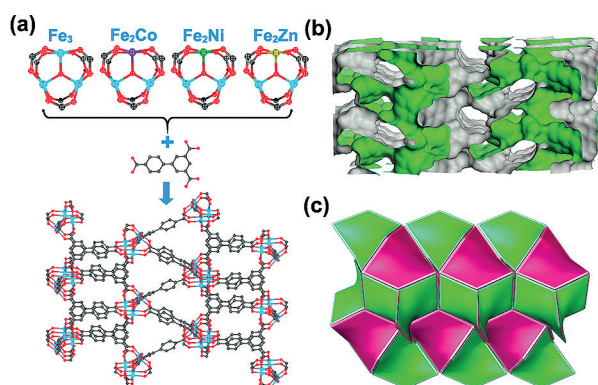


Figure 1. a) 3D framework of **NNU-21–24** connected by trinuclear metal clusters and tridentate carboxylate ligand. b) 3D channel simulated diagram of **NNU-23**. c) The natural tiling of **NNU-23**.

(Supporting Information, Figure S7). The textural porosity was determined by N_2 adsorption–desorption isotherms, where all the curves exhibit the typical type-I isotherms with a sharp nitrogen uptake at low relative pressure (Supporting Information, Figure S8), evidencing microporous characteristics of **NNU-21–24**. After N_2 adsorption–desorption measurement, the images of **NNU-21–24** (Supporting Information, Figure S10) are almost unchanged compared with those of as-synthesized MOFs. Notably, the N_2 adsorption–desorption isotherms exhibit no pronounced difference before and after stability test in 0.1M KOH (Supporting Information, Figure S11). These results further indicate the excellent stability of **NNU-21–24**. The water vapor adsorption isotherms measured at 298 K (Supporting Information, Figure S12) suggest that the channels of **NNU-21–24** can adsorb water vapor, which may contribute to the full contacts between active sites and electrolyte solution.

The electrocatalytic activity of **NNU-21–24** towards OER under 0.1M KOH was evaluated using a typical three-electrode system, where carbon cloth (CC) was modified with catalysts by drop-casting method and used as the working electrode directly (see the Experimental Section in the Supporting Information). Acetylene black (AB) was introduced to mix with the as-synthesized MOFs to improve the conductivity. The optimal mass ratio between MOFs and AB and the appropriate loading of catalysts were determined according to **NNU-23** (Supporting Information, Figures S13, S14).^[19] The optimal mass ratio and loading (that is, 1:1 and 1 mg cm^{-2}) are then used in the following experiments. For comparison, commercial IrO_2 was also examined under the same condition. According to the linear sweep voltammetry (LSV) curves (Figure 3a), **NNU-22**, **NNU-23**, and **NNU-24** exhibit more negative potential and higher current density in comparison with **NNU-21**. The Tafel slopes derived from the LSV curves are also analyzed in Figure 3b. The corresponding Tafel slopes for IrO_2 , **NNU-21**, **NNU-22**, **NNU-23**, **NNU-24** are 83.0 mV dec^{-1} , 122.7 mV dec^{-1} , 77.2 mV dec^{-1} , 81.8 mV dec^{-1} and 121.8 mV dec^{-1} , respectively, demonstrat-

ing the more effective kinetics of bimetallic electrocatalysts in OER.

Furthermore, the electrocatalytic performance of MOFs was compared by recording their overpotential at a current density of 10 mA cm^{-2} (η_{10}).^[20] As presented in Figure 3c, **NNU-23** displays an overpotential of 365 mV, which is lower than those of **NNU-21** (555 mV), **NNU-22** (376 mV), **NNU-24** (522 mV), and IrO_2 (390 mV). Besides, the overpotential of **NNU-23** is also one of the best among the reported MOF-based electrocatalysts in 0.1M KOH (Supporting Information, Table S4). We also calculated the electrochemical double-layer capacitance (C_{dl}) by measuring cyclic voltammetry (CV) curves to evaluate the electrochemical active surface area (ECSA).^[21] Clearly, **NNU-23** has the largest C_{dl} (5.10 mF cm^{-2}), and the C_{dl} values of bimetallic MOFs (that is, **NNU-22** (3.35 mF cm^{-2}), **NNU-23** (5.10 mF cm^{-2}), and **NNU-24** (2.69 mF cm^{-2})) are superior to that of monometallic MOF (that is, **NNU-21** (2.48 mF cm^{-2}); Figure 3d; Supporting Information, Figure S15). The C_{dl} results suggest that bimetallic Fe_2M MOFs have larger ECSA than monometallic Fe_3 MOFs when used as alkaline OER electrocatalysts. CV curves measured with a scan rate of 5 mV s^{-1} under a wider potential window are displayed in the Supporting Information, Figure S16. To study the electrode reaction kinetics, electrochemical impedance spectroscopy (EIS) of different samples were performed at the potential of 1.6 V vs. RHE.^[22] As revealed by the Nyquist plots (Supporting Information, Figure S17a) of the catalysts and corresponding equivalent circuit model (Supporting Information, Figure S17b), the charge transfer resistance (R_{ct}) of **NNU-22** ($8.48\text{ }\Omega$), **NNU-23** ($4.183\text{ }\Omega$), and **NNU-24** ($68.75\text{ }\Omega$) are significantly lower than that of **NNU-21** ($77.45\text{ }\Omega$), indicating the fastest charge transfer rate on the bimetallic Fe_2M MOFs, that results in the enhancement of the electrocatalytic performance for OER.

The long-term stability is another crucial criterion to evaluate electrocatalysts for applicability.^[14b,23] For **NNU-21–24**, the stability is assessed with CV and chronopotentiometric curves. As shown in the Supporting Information, Figure S18, all the subsequent LSV curves of the catalysts exhibit nearly no difference compared with the initial one after 2000 cycles. The chronopotentiometric curves (Supporting Information, Figure S19) also keep unchanged without degradation up to 15 h. These results demonstrate the high stability of the as-synthesized **NNU-21–24** during the long-term OER process.

To further explore the enhanced OER performance of various bimetallic MOFs, we performed spin-polarized density functional theory (DFT) calculations, which are represented by the simplified Fe_2M clusters (Figure 4a). As a benchmark, the Gibbs free energy (ΔG) diagrams of OER for the Fe_3 cluster, which can be determined using the adsorption free energies of O^* , OH , OH^* intermediate species, were firstly plotted by employing the computational hydrogen electrode (CHE) model (Further computational details are described in Supporting Information). As shown in Figure 4b, the rate-determining step (RDS) of Fe_3 cluster is the conversion of OH^* to O^* (with a considerably high overpotential of 1.03 V), which is essentially caused by the weak adsorption of O^* intermediate on Fe site ($\Delta G_{\text{O}^*} =$

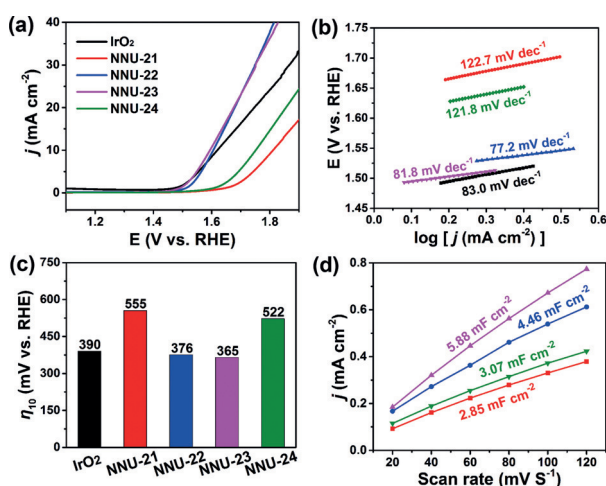


Figure 3. a) LSV curves and b) corresponding Tafel plots of IrO_2 and **NNU-21–24** for OER in 0.1 M KOH. c) A comparison of the overpotential at current density of 10 mA cm^{-2} . d) Plots used for evaluating the C_{dl} of **NNU-21–24**.

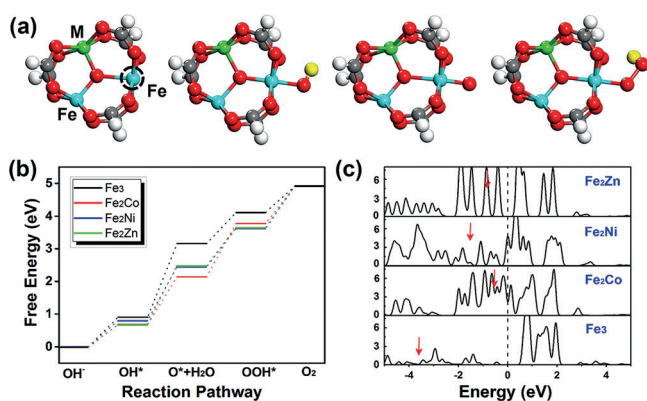


Figure 4. a) Initial structure of the Fe₂M cluster, followed by the adsorption of OH*, O*, and OOH* intermediates on the Fe site. The active site is marked by a dashed circle. b) The free energy profile for the OER pathway and c) projected density of states of Fe₂M-cluster. Red arrows denoted the d-band center.

3.16 eV). Therefore, it is expected that the overpotential can be lowered by strengthening the O* adsorption.

Next, we examined the effects of Co, Ni and Zn incorporation on OER activity of Fe₃ cluster. For each Fe₂M cluster, both Fe and the doped M sites were considered and we found that Fe atoms show better OER catalytic activity than the second M atoms for all three systems. Therefore, only the free energy curves of Fe sites were plotted in Figure 4 (those of M sites are plotted in the Supporting Information, Figure S20). The adsorption of O*, OH, and OOH* on the Fe site of Fe₂M clusters we calculated are all significantly enhanced compared to those of Fe₃ cluster (Supporting Information, Figure S21, Table S5). The ΔG_{O^*} of Fe site is significantly lowered to 2.15, 2.45, and 2.49 eV in Fe₂Co, Fe₂Ni, and Fe₂Zn, respectively. In particular, owing to relatively weak adsorption of OOH* species, the RDS of Fe₂Co cluster becomes the conversion of O* to OOH*. Overall, the OER overpotential of Fe₂Co (0.41 V), Fe₂Ni (0.42 V), and Fe₂Zn (0.59 V) clusters are significantly lower than that of Fe₃ cluster. Our calculations show that bimetallic clusters exhibit a pronouncedly improved OER catalytic performance, which is in good agreement with the experimental measurements.

To get some deep insights, we also plotted the partial density of states of metal atoms of various Fe₂M clusters. The position of d-band center for each cluster is also labeled. As shown in Figure 4c, the d-band center of the Fe₂Co, Fe₂Ni, and Fe₂Zn cluster are closer to the Fermi level than that of Fe₃ cluster. According to the d-band theory, a higher lying of d-band center would lead to stronger binding interaction between the adsorbates and catalyst, which essentially contributes to the enhancement of OER activity of Fe₂M clusters.

We also employed turnover frequency (TOF) to evaluate the intrinsic activity of NNU-21–24 based on the theoretical calculation results. Both Fe and M atom are regarded as active sites in NNU-21–24. The plots of TOF vs. potential for NNU-21–24 are shown in the Supporting Information, Figure S22a. With an overpotential of 400 mV applied (Supporting Information, Figure S22b), the TOF value of NNU-23 is the

highest among NNU-21–24. Besides, the TOF values of NNU-22 (0.028 s⁻¹), NNU-23 (0.030 s⁻¹) and NNU-24 (0.004 s⁻¹) are apparently higher than that of NNU-21 (0.002 s⁻¹), further confirming the excellent OER performance of the bimetallic catalysts.

In summary, we proposed a model of bimetallic electrocatalysts affecting their OER performance through both experimental results and theoretical computation utilizing the structural similarity between Fe₂M clusters and bimetallic electrocatalysts. We designed and synthesized a series of MOFs and employed them as electrochemical catalysts for OER. Among these MOFs, NNU-23 exhibits the best OER performance with an overpotential of 365 mV at 10 mA cm⁻², outperforming most previously reported MOF-based OER electrocatalysts in 0.1 M KOH. Notably, all examined bimetallic MOFs present better OER performance compared with monometallic MOFs. The DFT calculation reveals that the second metal can result in the d-band center close to Fermi level, and form a stronger binding interaction between the adsorbates and catalysts, thus improving the OER performance.

Acknowledgements

This work was supported by NSFC (No. 21622104, 21471080, and 21701085), the NSF of Jiangsu Province of China (No. BK20171032), the Natural Science Research of Jiangsu Higher Education Institutions of China (No. 17KJB150025), Priority Academic Program Development of Jiangsu Higher Education Institutions, and the Foundation of Jiangsu Collaborative Innovation Center of Biomedical Functional Materials.

Conflict of interest

The authors declare no conflict of interest.

Keywords: bimetallic electrocatalysts · clusters · iron · metal-organic frameworks · oxygen evolution reaction

How to cite: *Angew. Chem. Int. Ed.* **2018**, *57*, 9660–9664
Angew. Chem. **2018**, *130*, 9808–9812

- [1] a) Y. Jiao, Y. Zheng, M. Jaroniec, S. Z. Qiao, *Chem. Soc. Rev.* **2015**, *44*, 2060–2086; b) B. Y. Xia, Y. Yan, N. Li, H. B. Wu, X. W. Lou, X. Wang, *Nat. Energy* **2016**, *1*, 15006; c) C. Costentin, M. Robert, J.-M. Saveant, *Chem. Soc. Rev.* **2013**, *42*, 2423–2436; d) C. Spöri, J. T. H. Kwan, A. Bonakdarpour, D. P. Wilkinson, P. Strasser, *Angew. Chem. Int. Ed.* **2017**, *56*, 5994–6021; *Angew. Chem.* **2017**, *129*, 6088–6117.
- [2] a) Y. Zhao, R. Nakamura, K. Kamiya, S. Nakanishi, K. Hashimoto, *Nat. Commun.* **2013**, *4*, 2390; b) J. Suntivich, K. J. May, H. A. Gasteiger, J. B. Goodenough, Y. Shao-Horn, *Science* **2011**, *334*, 1383; c) P. Wang, M. Yan, J. Meng, G. Jiang, L. Qu, X. Pan, J. Z. Liu, L. Mai, *Nat. Commun.* **2017**, *8*, 645.
- [3] a) H. A. Bandal, A. R. Jadhav, A. H. Tamboli, H. Kim, *Electrochim. Acta* **2017**, *249*, 253–262; b) Y. Xiao, P. Zhang, X. Zhang, X. Dai, Y. Ma, Y. Wang, Y. Jiang, M. Liu, Y. Wang, *J. Mater. Chem. A* **2017**, *5*, 15901–15912.

- [4] a) M. S. Burke, L. J. Enman, A. S. Batchellor, S. Zou, S. W. Boettcher, *Chem. Mater.* **2015**, *27*, 7549–7558; b) X. Zou, Y. Liu, G.-D. Li, Y. Wu, D.-P. Liu, W. Li, H.-W. Li, D. Wang, Y. Zhang, X. Zou, *Adv. Mater.* **2017**, *29*, 1700404.
- [5] a) T. Zhang, J. Du, P. Xi, C. Xu, *ACS Appl. Mater. Interfaces* **2017**, *9*, 362–370; b) S. Fu, C. Zhu, J. Song, M. H. Engelhard, X. Li, D. Du, Y. Lin, *ACS Energy Lett.* **2016**, *1*, 792–796.
- [6] M. Shen, C. Ruan, Y. Chen, C. Jiang, K. Ai, L. Lu, *ACS Appl. Mater. Interfaces* **2015**, *7*, 1207–1218.
- [7] J. Hou, Y. Sun, S. Cao, Y. Wu, H. Chen, L. Sun, *ACS Appl. Mater. Interfaces* **2017**, *9*, 24600–24607.
- [8] R. D. L. Smith, C. Pasquini, S. Loos, P. Chernev, K. Klingan, P. Kubella, M. R. Mohammadi, D. Gonzalez-Flores, H. Dau, *Nat. Commun.* **2017**, *8*, 2022.
- [9] a) X.-F. Lu, P.-Q. Liao, J.-W. Wang, J.-X. Wu, X.-W. Chen, C.-T. He, J.-P. Zhang, G.-R. Li, X.-M. Chen, *J. Am. Chem. Soc.* **2016**, *138*, 8336–8339; b) T. Zhang, W. Lin, *Chem. Soc. Rev.* **2014**, *43*, 5982–5993; c) J.-S. Qin, D.-Y. Du, W. Guan, X.-J. Bo, Y.-F. Li, L.-P. Guo, Z.-M. Su, Y.-Y. Wang, Y.-Q. Lan, H.-C. Zhou, *J. Am. Chem. Soc.* **2015**, *137*, 7169–7177; d) N. Kornienko, Y. Zhao, C. S. Kley, C. Zhu, D. Kim, S. Lin, C. J. Chang, O. M. Yaghi, P. Yang, *J. Am. Chem. Soc.* **2015**, *137*, 14129–14135; e) P.-Q. Liao, J.-Q. Shen, J.-P. Zhang, *Coord. Chem. Rev.* **2017**, <https://doi.org/10.1016/j.ccr.2017.09.001>; f) F.-L. Li, Q. Shao, X. Huang, J.-P. Lang, *Angew. Chem. Int. Ed.* **2018**, *57*, 1888–1892; *Angew. Chem.* **2018**, *130*, 1906–1910; g) J. Duan, S. Chen, C. Zhao, *Nat. Commun.* **2017**, *8*, 15341; h) E. M. Miner, T. Fukushima, D. Sheberla, L. Sun, Y. Surendranath, M. Dincă, *Nat. Commun.* **2016**, *7*, 10942; i) M. Lions, J. B. Tommasino, R. Chattot, B. Abeykoon, N. Guillou, T. Devic, A. Demessence, L. Cardenas, F. Maillard, A. Fateeva, *Chem. Commun.* **2017**, *53*, 6496–6499.
- [10] J.-P. Zhang, Y.-B. Zhang, J.-B. Lin, X.-M. Chen, *Chem. Rev.* **2012**, *112*, 1001–1033.
- [11] D.-Y. Du, J.-S. Qin, S.-L. Li, Z.-M. Su, Y.-Q. Lan, *Chem. Soc. Rev.* **2014**, *43*, 4615–4632.
- [12] a) M. Bosch, M. Zhang, H.-C. Zhou, *Adv. Chem.* **2014**, 182327–182335; b) J. J. Low, A. I. Benin, P. Jakubczak, J. F. Abrahamian, S. A. Faheem, R. R. Willis, *J. Am. Chem. Soc.* **2009**, *131*, 15834–15842.
- [13] a) D. Feng, K. Wang, Z. Wei, Y.-P. Chen, C. M. Simon, R. K. Arvapally, R. L. Martin, M. Bosch, T.-F. Liu, S. Fordham, D. Yuan, M. A. Omary, M. Haranczyk, B. Smit, H.-C. Zhou, *Nat. Commun.* **2014**, *5*, 5723; b) T. Devic, C. Serre, *Chem. Soc. Rev.* **2014**, *43*, 6097–6115.
- [14] a) F. Lu, M. Zhou, Y. Zhou, X. Zeng, *Small* **2017**, *13*, 1701931; b) L. Han, S. Dong, E. Wang, *Adv. Mater.* **2016**, *28*, 9266–9291; c) V. S. Thoi, Y. Sun, J. R. Long, C. J. Chang, *Chem. Soc. Rev.* **2013**, *42*, 2388–2400.
- [15] a) J.-Q. Shen, P.-Q. Liao, D.-D. Zhou, C.-T. He, J.-X. Wu, W.-X. Zhang, J.-P. Zhang, X.-M. Chen, *J. Am. Chem. Soc.* **2017**, *139*, 1778–1781; b) G. Hai, X. Jia, K. Zhang, X. Liu, Z. Wu, G. Wang, *Nano Energy* **2018**, *44*, 345–352; c) L. Wang, Y. Wu, R. Cao, L. Ren, M. Chen, X. Feng, J. Zhou, B. Wang, *ACS Appl. Mater. Interfaces* **2016**, *8*, 16736–16743.
- [16] S. Wongsakulphasatch, F. Nouar, J. Rodriguez, L. Scott, C. Le Guillouzer, T. Devic, P. Horcajada, J. M. Greneche, P. L. Llewellyn, A. Vimont, G. Clet, M. Daturi, C. Serre, *Chem. Commun.* **2015**, *51*, 10194–10197.
- [17] E. V. Alexandrov, V. A. Blatov, A. V. Kochetkov, D. M. Proserpio, *CrystEngComm* **2011**, *13*, 3947–3958.
- [18] A. Spek, *Acta Crystallogr. Sect. D* **2009**, *65*, 148–155.
- [19] P. Chakthranont, J. Kibsgaard, A. Gallo, J. Park, M. Mitani, D. Sokaras, T. Kroll, R. Sinclair, M. B. Mogenssen, T. F. Jaramillo, *ACS Catal.* **2017**, *7*, 5399–5409.
- [20] a) L.-L. Feng, G. Yu, Y. Wu, G.-D. Li, H. Li, Y. Sun, T. Asefa, W. Chen, X. Zou, *J. Am. Chem. Soc.* **2015**, *137*, 14023–14026; b) S. Zhao, R. Jin, H. Abroshan, C. Zeng, H. Zhang, S. D. House, E. Gottlieb, H. J. Kim, J. C. Yang, R. Jin, *J. Am. Chem. Soc.* **2017**, *139*, 1077–1080.
- [21] a) P. He, X.-Y. Yu, X. W. Lou, *Angew. Chem. Int. Ed.* **2017**, *56*, 3897–3900; *Angew. Chem.* **2017**, *129*, 3955–3958; b) F. Hu, S. Zhu, S. Chen, Y. Li, L. Ma, T. Wu, Y. Zhang, C. Wang, C. Liu, X. Yang, L. Song, X. Yang, Y. Xiong, *Adv. Mater.* **2017**, *29*, 1606570.
- [22] Y.-J. Tang, M.-R. Gao, C.-H. Liu, S.-L. Li, H.-L. Jiang, Y.-Q. Lan, M. Han, S.-H. Yu, *Angew. Chem. Int. Ed.* **2015**, *54*, 12928–12932; *Angew. Chem.* **2015**, *127*, 13120–13124.
- [23] X.-F. Lu, L.-F. Gu, J.-W. Wang, J.-X. Wu, P.-Q. Liao, G.-R. Li, *Adv. Mater.* **2017**, *29*, 1604437.

Manuscript received: March 26, 2018

Accepted manuscript online: April 16, 2018

Version of record online: May 3, 2018